Energy Reports 8 (2022) 3649–3660

Contents lists available at ScienceDirect

Energy Reports

journal homepage: www.elsevier.com/locate/egyr

Alloy selections in high-temperature metal hydride heat pump systems for industrial waste heat recovery

Y.T. Ge *, P.Y. Lang

School of the Built Environment and Architecture, London South Bank University, 103 Borough Road, London, SE1 0AA, UK

ARTICLE INFO

Article history:
Received 20 December 2021
Received in revised form 12 February 2022
Accepted 23 February 2022
Available online xxxx

Keywords:
Waste heat recovery
High-temperature metal hydride (MH) heat pumps
Alloy selections
System efficiencies

ABSTRACT

In an energy intensive industrial site such as a steel plant, there are plenty of medium and low temperature waste heat which could be recovered for heating purposes with advanced and feasible technologies for example metal hydride (MH) heat pumps. Compared to other heat pump systems such as those with compression and absorption cycles, the MH heat pump has some distinctive advantages including low carbon system in terms of less electricity input and environmentally friendly working mediums, compactness, and most importantly achievable heat output with relatively high temperature. However, the applicable alloys for the high-temperature MH heat pump systems are critical and need to be purposely selected. Accordingly, in this paper, a comprehensive procedure to select alloys for the high-temperature MH heat pump systems is explained based on the operating temperatures, system efficiencies and thermodynamic equilibriums. From the database of literatures, totally 82 alloys are potentially used for this special application of which 1560 alloy pairs are formed and each pair consists of one high-temperature alloy and another low-temperature alloy. Subsequently, a number of applicable alloys are selected for each designed temperature of heat pump output and one pair is ultimately finalised. The alloy can be further examined considering of its thermophysical properties, heat transfer behaviours, costs and safety issues.

Contents

1. Introduction

Industrial waste heat recovery for decarbonised heating and cooling is an attractive concept that could simultaneously reduce fossil fuel consumption and CO_2 emissions. In the UK, based on a recent report, of the total industrial waste heat sources, about 28 TWh/yr could be potentially used in district heat networks (Anon, 2014). The waste heat sources from different industrial sectors can have different temperature grades and various applications. For the low grade heat sources with temperature below 230 °C, Organic Rankine Cycles (ORCs) might be applied for potential power generations. However, the thermal (electric) efficiency of an ORC with the low grade heat source is quite low (about 10% or below) which might not be a good investment from the economic point of view (L. Li et al., 2017). In addition, a typical energy intensive industrial site such as steel plant also has plenty of waste heat with extra low grade around 40 °C which is conventionally exhaust to ambient directly (Patsos, 2010). These low grade waste heat sources can be combined with some advanced energy conversion systems such as heat pump to produce average low grade heat sources at temperature around 130 °C which

* Corresponding author.
E-mail address: yunting.ge@lsbu.ac.uk (Y.T. Ge).

https://doi.org/10.1016/j.egyr.2022.02.279

Nomenclature

C_v	specific heat at constant volume (J/mol alloy K)
C_p	specific heat at constant pressure (J/kg K)
COA	coefficient of amplification
ΔH	standard enthalpy (kJ/mol H_2)
HT	high temperature
LT	low temperature
n	molar number
P	pressure (atm)
Q	heat capacity (W or kW)
R	universal gas constant
ΔS	standard enthalpy and entropy (J/mol H_2 K)
T	Temperature (K)
W	Weight (kg)
WM	molar weight (g/mol)
ψ	exergy efficiency

Subscripts

c	Carnot
h	high
l	low
m, MH	metal hydride
R	reactor
t	transfer
1	reactor one
2	reactor 2

are more applicable for district heating at remote areas. Correspondingly, the conventional absorption or adsorption heat pump systems might be applied but they are hard to obtain heat output with temperature as high as 130 °C. Alternatively, a hydrogen related technology namely metal hydride (MH) heat pump can be a feasible option to achieve a high temperature heat output. Its working mechanism is quite similar to that of absorption or adsorption heat pump. However, for a MH heat pump, high and low temperature metal hydride alloys and hydrogen working fluid are applied to absorb heat from high and low temperature heat resources and produce heat at medium temperature. Meanwhile, the hydrogen desorption and absorption processes are conducted respectively during the heat input and output operations. Comparing to absorption or adsorption heat pump, the MH heat pump has similar operation efficiency but is more compact and can achieve higher temperature heat output. The MH heat pump has been investigated mostly in conventional heat pump systems (Gamnini, 1989; Bjurstrom and Suda, 1989), but has not been applied in district heating systems with industrial waste heat due to relatively high temperature heat input and output. To facilitate this, one of the critical points is to select appropriate alloy pairs for the MH heat pump at the applicable operating conditions and acceptable system performance efficiency.

Conventionally, the applicable alloys for the MH heat pump (MHHP) systems are categorised as intermetallics with conventions of AB, AB_2, A_2B and AB_5, where 'A' is usually a lanthanide element (Atomic numbers 57–71), such as La, or mischmetal (rare earth metal mixture), and 'B' is Ni, Co, Al, Mn, Fe, Sn, Cu, Ti etc. (D. Chandra et al., 2006). In addition, element 'A' refers to rare earth and alkaline elements, presenting a high affinity for hydrogen to form stable hydride, while element 'B' is generally a transition metal and it usually presents a poor affinity for hydrogen and thus forming unstable hydrides (Payá Herrero, 2010). The A_xB_y alloys can be modified by changing the alloy composition of *x* or *y* such that metal hydride with suitable properties can be formed (Nakamura et al., 1997; Muthukumar and Groll, 2010). Therefore, plenty of such alloys have been synthesised, characterised and are recommended for use in MHHPs. In addition, these intermetallic materials can be used as either low or high temperature alloys in their associated heat pump systems based on their corresponding operating temperatures and pressures. Satheesh and Muthukumar (2010) investigated a single-stage metal hydride heat pump working with five different alloy pairs of AB_5, AB_2, AB types of alloys. These included $MmNi_{4.6}Al_{0.4}$/$MmNi_{4.6}Fe_{0.4}$, $LaNi_{4.61}Mn_{0.26}Al_{0.13}$/$La_{0.6}Y_{0.4}Ni_{4.8}Mn_{0.2}$, $LmNi_{4.91}Sn_{0.15}$/$Ti_{0.99}Zr_{0.01}V_{0.43}Fe_{0.09}Cr_{0.05}Mn_{1.5}$, $LaNi_{4.6}Al_{0.4}$/$MmNi_{4.15}Fe_{0.85}$ and $Zr_{0.9}Ti_{0.1}Cr_{0.9}Fe_{1.1}$/$Zr_{0.9}Ti_{0.1}Cr_{0.6}Fe_{1.4}$. The high ($T_H$), medium ($T_M$) and low ($T_L$) MH temperatures in the system were in the ranges of 110∼170 °C, 25∼35 °C and -30∼20 °C respectively, while the high and low operating pressures were in the ranges of 30∼40 bar and 0.1∼2 bar each. Based on the calculated system COP with each alloy pair, the optimum operating temperature ranges of each pair were suggested. At a heat source temperature of 130 °C and a refrigeration temperature of 20 °C, a single-stage MHHP working with $LmNi_{4.91}Sn_{0.15}$/ $Ti_{0.99}Zr_{0.01}V_{0.43}Fe_{0.09}Cr_{0.05}Mn_{1.5}$ was investigated numerically and experimentally (Linder and Laurien, 2009). The COP was calculated as 0.25 which was relatively low. A MHHP with $MmNi_{4.5}Al_{0.5}$/$MmNi_{4.2}Al_{0.1}Fe_{0.7}$ MH alloy pair was studied theoretically by Mellouli et al. (2009). For the operating temperature ranges of 52∼167 °C/0∼20 °C/-23∼-8 °C (TH/TM/TL), the COP was calculated as 0.45∼0.5. There are also some other research investigations from literatures on MHHPs (Qin et al., 2007; Ni and Liu, 2007; Lee et al., 1995). The heat source temperature can be as high as 200 °C but the heat output temperatures are mostly below 50 °C. If a MHHP is applied for space heating purpose, a higher heat output temperature up to 100 °C is required. In addition, for the applications of industrial processes, the heat output temperature from the heat pump up to 150 °C is expected (George et al., 2020). However, such a high temperature is hard to be achieved with conventional compression and absorption heat pumps. Potentially, the MHHPs can obtain the heat output with such a high temperature but the applied MH alloys should be purposely selected, which have not been done yet from literatures.

Subsequently, in this paper, a comprehensive procedure to select alloys for the high-temperature MH heat pump systems is explained based on the operating temperatures, system efficiencies and thermodynamic equilibriums. From the database of literatures, totally 82 alloys are potentially used for this special application of which 1560 alloy pairs are formed and each pair consists of one high-temperature alloy and another low-temperature alloy. Subsequently, a number of applicable alloys are selected for each designed temperature of heat pump heat output. An applicable MH alloy pair is thus finalised based on its operating pressures and performance efficiencies.

2. System description

The schematic diagram of the MHHP system and its operating cycle on a Van't Hoff plot is shown in Fig. 1. As depicted, the system consists of two MH reactor pairs, MH1a and MH2a, and MH1b and MH2b. Each pair has one high temperature MH reactor (MH1a or MH1b) and one low temperature MH reactor (MH2a or MH2b). For each MH reactor pair, a hydrogen connection pipe with a control valve is connected in-between to facilitate hydrogen to flow between two reactors. In the system, there are one heat input (Q_h) with high temperature (T_h), one heat input (Q_l)

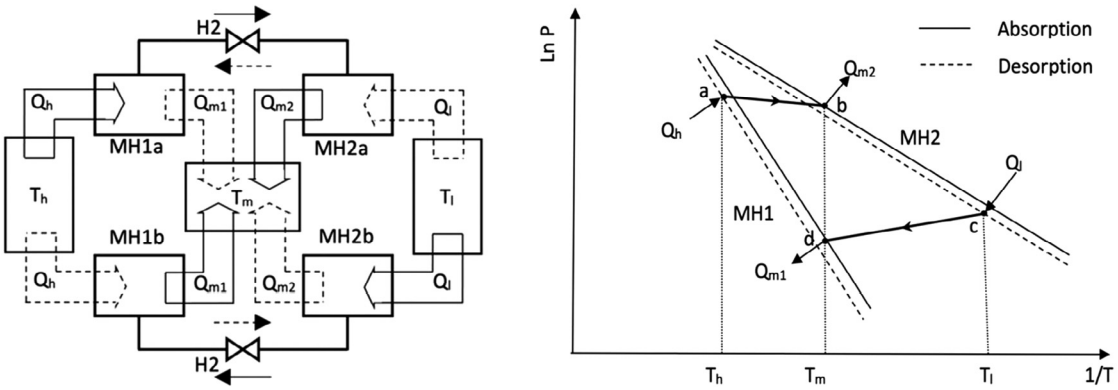

Fig. 1. Schematic diagram of a single stage metal hydride heat pump and its operating cycle on a Van't Hoff plot . (Q_h =heat input at high temperature heat source T_h; Q_{m1},Q_{m2}=heat outputs at output temperature T_m; Q_l=Heat absorption at low temperature heat source T_l).

with low temperature (T_l), and two heat outputs (Q_{m1} and Q_{m2}) with medium temperature (T_m). The system operation consists of two half cycles. For the first half cycle (solid line in the system layout), the high temperature heat Q_h is input to MH1a such that hydrogen (H2) is desorbed from MH1a and passes through the H2 connection pipe and is absorbed by MH2a. The reaction heat Q_{m2} at temperature T_m during the absorption process is therefore released from MH2a. Meanwhile, the low temperature heat Q_l is added to MH2b to desorb H2 from the reactor. The H2 released from MH2b then passes through the H2 connection pipe and is absorbed by MH1b such that the heat Q_{m1} at temperature T_m is released. For the second half cycle (dot line in the system layout), the directions of heat inputs to and outputs from the reactors are swapped. In that case, Q_h and Q_l are inputs to MH1b and MH2a respectively while Q_{m1} and Q_{m2} are outputs from MH1a and MH2b each. In addition, the H2 flows in those two connection pipes flow in opposite directions to those in the first half cycle. The operating cycle can thus ensure continuous operation of the system. It should be noted that the temperatures of heat source (T_h and T_l) and heat sink (T_m) are assumed the same as those of their corresponding reactors.

3. MH alloy selection

3.1. Thermodynamic analysis

For the application of industrial waste heat recovery using the MHHP system described in Section 2, the designed temperature ranges of high temperature (T_h), medium temperature (T_m) and low temperature (T_l) heat sources are specified as 180∼240 °C, 120∼140 °C and 25∼45 °C respectively. For the hydrogen absorption or desorption process of a MH reactor in the system, the MH alloy (M) reacts reversibly with hydrogen (H_2) as follows:

$$M + (\frac{x}{2})H_2 \underset{desorption}{\overset{absorption}{\rightleftarrows}} MH_x + Q \tag{1}$$

where x is the hydrogen atom number in the metal hydride, Q is heat release during hydrogen absorption (exothermic) process or heat input during hydrogen desorption (endothermic) process. For each reaction process, the van't Hoff's law applies with following form:

$$\ln P_{H_2} = -\frac{\Delta H \times 1000}{RT} + \frac{\Delta S}{R} \tag{2}$$

where P_{H_2}(atm) is hydrogen pressure, ΔH (kJ/mol H_2) and ΔS (J/mol H_2.K) are the standard enthalpy and entropy of hydride formation respectively, R is the gas constant (8.134 J/mol.K) and T is the hydrogen temperature (K). This equation is schematically represented in Fig. 1 for both MH1 and MH2 with two reaction processes including desorption and absorption. For a particular MH, the ΔH and ΔS are fixed such that the hydrogen absorption or desorption pressure is a function of reactor or hydrogen temperature only. For this MHHP system, since the designed temperatures of T_h, T_m and T_l are specified, the corresponding hydrogen pressure P_h, P_{m1}, P_{m2} and P_l can be calculated with Eq. (2). P_{m1} and P_{m2} represent hydrogen pressures in MH1 and MH2 respectively at the same medium temperature T_m. As seen from Fig. 1, the system operates at two different pressure levels, high and low. At the high pressure level, the hydrogen with temperature T_h and pressure P_h is desorbed at MH1 and flows to MH2 at temperature T_m and pressure P_{m2} and is absorbed there. At the low pressure level, the hydrogen with temperature T_l and pressure P_l is desorbed at MH2 and flows to MH1 at temperature T_m and pressure P_{m1} and is absorbed there. Practically, to enable the hydrogen to flow from one reactor to another, the pressure P_h and P_l should be slightly higher than P_{m2} and P_{m1} respectively. However, to facilitate the MH alloy selection, P_h and P_l are assumed the same as P_{m2} and P_{m1} correspondingly. In that case, the following formulas will follow:

$$-\frac{\Delta H_1 \times 1000}{T_h} + \Delta S_1 = -\frac{\Delta H_2 \times 1000}{T_m} + \Delta S_2 \tag{3}$$

$$-\frac{\Delta H_1 \times 1000}{T_m} + \Delta S_1 = -\frac{\Delta H_2 \times 1000}{T_l} + \Delta S_2 \tag{4}$$

where, the subscripts 1 and 2 indicate the MH reactor 1 (MH1) and 2 (MH2) respectively. To simply, two parameters of η and ξ are defined as below:

$$\eta = \frac{\Delta S_1 - \Delta S_2}{\Delta H_2} \tag{5}$$

$$\xi = \frac{\Delta H_1}{\Delta H_2} \tag{6}$$

Accordingly, the following equations are obtained:

$$\eta = (\frac{\xi}{T_h} - \frac{1}{T_m}) \times 1000 \tag{7}$$

$$\eta = (\frac{\xi}{T_m} - \frac{1}{T_l}) \times 1000 \tag{8}$$

From Eqs. (5) and (6), the parameters η and ξ are the functions of thermophysical properties of the MH alloy pair applied particularly the values of their ΔH and ΔS. Based on Eqs. (7) and (8), the parameters η and ξ are also constrained by the operating temperatures of T_h, T_m and T_l. Therefore, at specified temperature ranges of T_h, T_m and T_l, the potential MH alloy pairs used in the MHHP system can be identified. From literature review, as listed in Table 1, totally 82 MH alloys are chosen

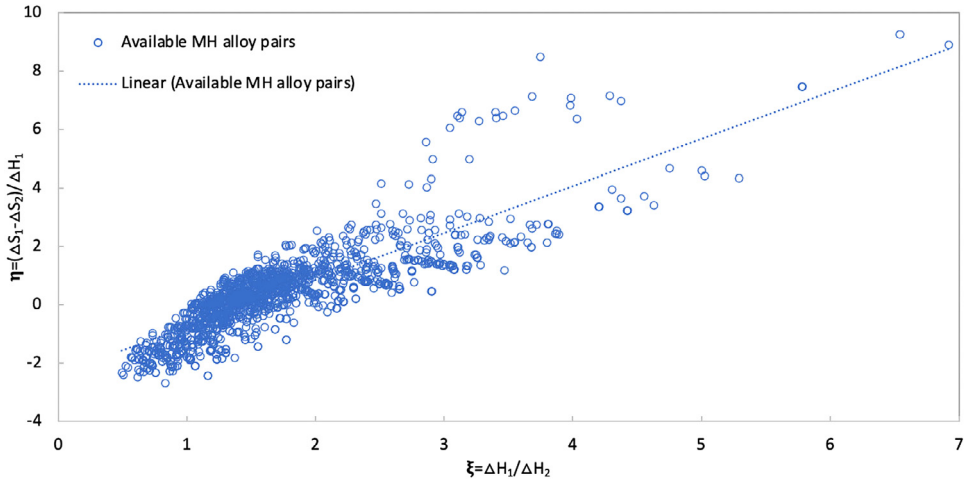

Fig. 2. Coordinate points (ξ, η) for all the available MH alloy pairs.

from which the potential MH alloy pairs for the MHHP system will be selected (Satheesh and Muthukumar, 2010; Dantzer and Orgaz, 1986; Huston, 1980; Kim et al., 1997; Yasuda et al., 2013; Lototskyy et al., 2016; Qin et al., 2007b; Skripnyuk and Ron, 1999; Linder and Kulenovic, 2011; Rusman and Dahari, 2016; Weckerle et al., 2019). As listed in the table, the important parameters of ΔH and ΔS for each MH alloy are listed. In addition, for this particular MHHP, it is known that the lowest average MH reactor temperature T_l is 35 °C. Correspondingly, the hydrogen pressure P_l is calculated for each MH reactor. In the proposed system, it consists of two identical high temperature (HT) MH alloys and two identical low temperature (LT) MH alloys. Therefore, two types of MH alloys, HT and LT, need to be identified in the system. To classify, if the calculated P_l is less than 1 bar, the MH alloy is HT one otherwise it is LT one. Subsequently, of the total 82 MH alloys, 30 are classified as HT types and 52 are belonged to LT alloys. For each HT MH alloy, it can be paired with any of the LT MH alloys such that totally 1560 MH pairs can be formed.

Based on the Eqs. (5) and (6), the coordinate points (ξ, η) of all the available MH alloy pairs (1560 in total) can be demonstrated in a $\xi - \eta$ diagram, as shown in Fig. 2. From this statistical diagram, it can see roughly a linear relation between η and ξ although further verification is needed. In addition, according to Eqs. (7) and (8), at a constant T_h and T_m or constant T_l and T_m, a straight line of function $\eta(\xi)$ can be drawn. From the system design, the maximum and minimum values of T_h are set to 220 °C and 180 °C respectively, while the maximum and minimum values of T_l are set to 25 °C and 45 °C each. Therefore, at a constant T_m, four straight lines at the maximum and minimum values of T_h and T_l can be shown in the same diagram. Correspondingly, when temperatures of T_m are set to 120 °C, 130 °C and 140 °C coordinate points $(\boldsymbol{\xi}, \boldsymbol{\eta})$ for the available MH alloys and four straight lines at maximum and minimum temperatures of T_h and T_l are shown in Figs. 3–5 respectively. At a constant T_m, the system should operate with the temperatures of T_h and T_l at their respective temperature ranges. As such, the coordinate points $(\boldsymbol{\xi}, \boldsymbol{\eta})$ representing the applicable MH alloy pairs (solid circles in the diagram) should be enclosed with those four straight lines. Subsequently, there are 109, 35 and 12 applicable MH alloy pairs for T_m temperatures at 120 °C, 130 °C and 140 °C respectively. It can be seen that the higher the heat pump output temperature is the less the applicable MH alloy pairs would be. However, the applicable MH alloys need to be further evaluated and identified based on the system performance when these alloy pairs are applied.

It should be noted that due to the inherent hysteresis in a MH alloy, at a constant temperature the MH absorption pressure is higher than that of desorption pressure. However, to simplify the selection procedure, the effect of the hysteresis on the MH alloy selection is neglected. In a practical application, once the MH alloys are identified, the heat source and sink temperatures can always be adjusted slightly to meet the pressure difference requirement of hydrogen transfer between two reactors.

3.2. Operation analysis

To analyse the system performance at the specified operating condition and MH alloy pairs, the energy input or output from each MH reactor in the system shown in Fig. 1 needs to be identified and calculated. To achieve that, it is necessary to fully understand the system operating cycle and the role of each MH reactor. For the HT MH reactors MH1a and MH1b, one reactor receives heat Q_h and another releases heat Q_{m1} for the first half cycle while for the second half cycle, the roles of these two reactors are changed over. Similarly, for the LT MH reactors MH2a and MH2b, one reactor receives heat Q_l and another releases heat Q_{m2} for the first half cycle while for the second half cycle, the roles of these two reactors are swapped. In addition, the directions of hydrogen transports from one reactor to another also changed over between two half cycles. Subsequently, the Q_h, Q_{m1}, Q_{m2} and Q_l can be calculated by Eqs. (9) to (12) respectively.

$$Q_h = n_{t1}\Delta H_1 + (n_1 C v_1 + W_{1R} C p_{1R})(T_h - T_m) \quad (9)$$

$$Q_{m1} = n_{t2}\Delta H_1 + (n_1 C v_1 + W_{1R} C p_{1R})(T_h - T_m) \quad (10)$$

$$Q_{m2} = n_{t1}\Delta H_2 - (n_2 C v_2 + W_{2R} C p_{2R})(T_m - T_l) \quad (11)$$

$$Q_l = n_{t2}\Delta H_2 - (n_2 C v_2 + W_{2R} C p_{2R})(T_m - T_l) \quad (12)$$

In these equations, n_{t1} and n_{t2} are the total amount of hydrogen (mol) transferred from reactor MH1 and MH2 respectively, which should be the same at steady state. The n_{t1} or n_{t2} can be calculated based on the weight and gravimetric hydrogen storage capacity of respective metal hydride alloy charged in the reactor. The n_1 and n_2 are the number of moles of MH alloys for MH1 and MH2 respectively, which are dependent on the weight and type of MH alloy charged in each reactor. The W_{1R} and W_{2R} are the metal weight of reactor MH1 and MH2 respectively. The Cp_{1R} and Cp_{2R} are the specific heat capacity of metal reactor MH1 and MH2 respectively. It is noted that at the stage of MH alloy selection, the heat capacity rate of each reactor is not included in the energy calculation. However, these heat capacity rates should

Table 1
MH alloys to be selected.

No	Alloy	△H	△S	T_l	P_l	LT or HT	Ref
		kJ/mol H2	J/K/mol H2	°C	bar		
1	Mg(LaNis)20%	76.99	138.32	35	1.517E−06	HT	Dantzer and Orgaz (1986)
2	Mg_2Cu	72.80	142.34	35	1.258E−05	HT	Huston (1980)
3	Mg_2Ni	64.43	122.30	35	2.962E−05	HT	Huston (1980)
4	$Mg_{2.4}Ni$	64.31	122.30	35	3.111E−05	HT	Dantzer and Orgaz (1986)
5	$LaNi_{4.06}Mn_{0.94}$	48.70	116.90	35	7.186E−03	HT	Dantzer and Orgaz (1986)
6	$LaNi_4Al$	47.70	118.83	35	0.013	HT	Dantzer and Orgaz (1986)
7	$Z\ r_{0.8}Ce_{0.2}Mn_2$	44.89	110.00	35	0.014	HT	Dantzer and Orgaz (1986)
8	$LaNi_{4.30}Mn_{0.70}$	44.27	115.14	35	0.033	HT	Dantzer and Orgaz (1986)
9	NiZr	30.42	71.63	35	0.039	HT	Dantzer and Orgaz (1986)
10	$ZrMn_2Cu_{0.8}$	25.82	57.74	35	0.044	HT	Kim et al. (1997)
11	$LaNi_{4.25}Al_{0.75}$	44.35	117.99	35	0.045	HT	Dantzer and Orgaz (1986)
12	$ZrMn_2Cu_{0.8}$	25.82	57.91	35	0.045	HT	Dantzer and Orgaz (1986)
13	$TiFe_{\ 0.9}Ni_{0.1}$	35.60	94.65	35	0.082	HT	Yasuda et al. (2013)
14	$Zr_{0.7}Ti_{0.3}Mn_2$	32.30	87.36	35	0.124	HT	Dantzer and Orgaz (1986)
15	$LaNi_{4.56}Mn_{0.44}$	39.50	113.22	35	0.168	HT	Dantzer and Orgaz (1986)
16	$Fe_{0.8}Ni_{0.2}Ti$	41.00	118.81	35	0.182	HT	Huston (1980)
17	$LaNi_{4.5}Al_{0.5}$	38.49	111.29	35	0.197	HT	Dantzer and Orgaz (1986)
18	$LaNi_{4.61}Mn_{0.26}Al_{0.13}$	37.90	110.35	35	0.221	HT	Satheesh and Muthukumar (2010)
19	$LaNi_{4.61}Mn_{0.26}Al_{0.13}$	32.38	94.69	35	0.291	HT	Satheesh and Muthukumar (2010)
20	$LaNi_{4.65}Mn_{0.35}$	37.82	112.55	35	0.297	HT	Dantzer and Orgaz (1986)
21	$LaNi_{4.6}Al_{0.4}$	36.40	109.20	35	0.346	HT	Dantzer and Orgaz (1986)
22	$ZrMn_{\ 2.8}$	18.41	52.30	35	0.414	HT	Dantzer and Orgaz (1986)
23	$Zr_{0.9}Ti_{0.1}Cr_{0.9}Fe_{1.1}$	27.97	85.60	35	0.544	HT	Satheesh and Muthukumar (2010)
24	$LaNi_{4.7}Al_{0.3}$	33.89	106.75	35	0.687	HT	Huston (1980)
25	$ZrMn_{\ 3.8}$	19.71	61.50	35	0.755	HT	Dantzer and Orgaz (1986)
26	$LaNi_{4.75}Al_{0.25}$	34.73	110.46	35	0.774	HT	Dantzer and Orgaz (1986)
27	$CaNi_5$	31.80	101.18	35	0.796	HT	Huston (1980)
28	$V_{0.9}Cr_{0.1}$	41.71	133.89	35	0.848	HT	Kim et al. (1997)
29	$LaNi_{4.83}Mn_{0.17}$	34.52	111.25	35	0.924	HT	Dantzer and Orgaz (1986)
30	$LaNi_{4.8}Al_{0.2}$	34.90	112.65	35	0.942	HT	Lototskyy et al. (2016)
31	$LaNi_{4.6}Al_{0.4}$	30.68	99.73	35	1.034	LT	Satheesh and Muthukumar (2010)
32	$La_{0.6}Y_{0.4}Ni_{4.9}Al_{0.1}$	26.85	87.35	35	1.040	LT	Qin et al. (2007b)
33	$ZrCr_{\ 0.6}Fe_{1.4}$	26.90	89.50	35	1.319	LT	Dantzer and Orgaz (1986)
34	$Zr_{0.8}Ti_{0.2}$ MnFe	11.13	39.25	35	1.476	LT	Dantzer and Orgaz (1986)
35	$LaNi_{4.9}Al_{0.1}$	32.64	110.46	35	1.752	LT	Dantzer and Orgaz (1986)
36	$LaNi_{4.95}Mn_{0.05}$	32.30	110.37	35	1.976	LT	Dantzer and Orgaz (1986)
37	$LaNi_5$	31.80	110.04	35	2.309	LT	Dantzer and Orgaz (1986)
38	$Zr_{0.9}Ti_{0.1}Cr_{0.6}Fe_{1.4}$	23.61	85.23	35	2.860	LT	Satheesh and Muthukumar (2010)
39	$LmNi_{\ 4.91}Sn_{0.15}$	25.90	93.82	35	3.282	LT	Satheesh and Muthukumar (2010)
40	$MNi_{4.5}Al_{0.46}Fe_{0.05}$	31.05	110.88	35	3.426	LT	Kim et al. (1997)
41	$Zr(Fe_{0.75}Cr_{0.25})_2$	24.77	91.63	35	3.920	LT	Kim et al. (1997)
42	$La_{0.6}Y_{0.4}Ni_{4.8}Mn_{0.2}$	23.25	86.78	35	3.961	LT	Satheesh and Muthukumar (2010)
43	$Fe_{0.85}Mn_{0.15}Ti$	29.46	107.11	35	4.052	LT	Kim et al. (1997)
44	$Ce_{0.5}La_{0.5}Ni_{2.5}Cu_{2.5}$	23.01	86.61	35	4.255	LT	Kim et al. (1997)
45	$Fe_{0.9}Mn_{0.1}Ti$	29.29	107.00	35	4.269	LT	Huston (1980)
46	$La_{0.6}Y_{0.4}Ni_{4.8}Mn_{0.2}$	27.05	100.50	35	4.678	LT	Satheesh and Muthukumar (2010)
47	$Z\ r_{0.8}Ti_{0.2}Cr_{0.6}Fe_{1.4}$	26.90	100.46	35	4.929	LT	Dantzer and Orgaz (1986)
48	$Ca_{0.7}M_{0.3}Ni_5$	26.78	100.42	35	5.151	LT	Kim et al. (1997)
49	$Ca_{0.7}M_{0.3}Ni_5$	26.78	100.43	35	5.161	LT	Huston (1980)
50	$MmNi_{\ 4.6}Al_{0.4}$	24.68	93.82	35	5.278	LT	Satheesh and Muthukumar (2010)
51	$Ce_{1.1}Ni_{2.5}Cu_{2.5}$	20.71	81.04	35	5.350	LT	Dantzer and Orgaz (1986)
52	$MNi_{4.5}Al_{0.5}$	28.03	104.84	35	5.372	LT	Huston (1980)
53	$MNi_{4.5}Al_{0.05}$	28.03	105.44	35	5.772	LT	Kim et al. (1997)
54	FeTi	28.03	106.09	35	6.242	LT	Huston (1980)
55	$V_{0.95}Cr_{0.05}$	37.36	139.33	35	8.913	LT	Kim et al. (1997)
56	$Ca_{0.5}M_{0.5}Ni_5$	25.77	103.76	35	11.400	LT	Kim et al. (1997)
57	$CeNi_{\ 2.5}Cu_{2.5}$	16.90	75.31	35	11.867	LT	Dantzer and Orgaz (1986)
58	$MmNi_{\ 4.6}Fe_{0.4}$	21.68	91.22	35	12.432	LT	Satheesh and Muthukumar (2010)
59	$CeNi_3Cu_2$	15.31	70.58	35	12.500	LT	Dantzer and Orgaz (1986)
60	$CeNi_{\ 4.5}Al_{0.5}$	21.88	92.05	35	12.722	LT	Kim et al. (1997)
61	$Ti_{0.95}Zr_{0.05}Mn_{1.48}V_{0.43}Fe_{0.08}Al_{0.01}$	25.35	103.65	35	13.267	LT	Skripnyuk and Ron (1999)
62	$Ti_{0.95}Zr_{0.05}Mn_{1.46}V_{0.45}Fe_{0.09}$	25.26	103.55	35	13.578	LT	Linder and Kulenovic (2011)
63	$MmNi_{\ 4.15}Fe_{0.85}$	21.73	92.13	35	13.641	LT	Satheesh and Muthukumar (2010)
64	$V_{0.925}Cr_{0.075}$	36.32	139.75	35	14.099	LT	Kim et al. (1997)
65	$CeNi_3Zr_2$	29.55	118.25	35	14.897	LT	Rusman and Dahari (2016)
66	$MNi_{4.15}Fe_{0.85}$	25.10	104.60	35	16.372	LT	Kim et al. (1997)
67	$MNi_{4.15}Fe_{0.85}$	25.10	104.76	35	16.683	LT	Huston (1980)
68	$Ca_{0.4}M_{0.6}Ni_5$	25.27	105.44	35	16.961	LT	Kim et al. (1997)
69	$Ti_{0.98}Zr_{0.02}V_{0.41}Fe_{0.09}Cr_{0.05}Mn_{1.46}$	19.85	87.85	35	16.974	LT	Weckerle et al. (2019)
70	$CeNi_4Zr$	21.08	93.30	35	20.220	LT	Rusman and Dahari (2016)
71	$PrNi_5$	29.04	119.24	35	20.529	LT	Kim et al. (1997)
72	$NdNi_5$	27.82	116.32	35	23.177	LT	Kim et al. (1997)
73	$Ti_{0.99}Zr_{0.01}V_{0.43}Fe_{0.09}Cr_{0.05}Mn_{1.5}$	19.77	90.35	35	23.620	LT	Linder and Kulenovic (2011)

(*continued on next page*)

Table 1 (*continued*).

No	Alloy	△H	△S	T_l	P_l	LT or HT	Ref
		kJ/mol H2	J/K/mol H2	°C	bar		
74	$CeNi_4Cr$	16.63	81.59	35	28.095	LT	Rusman and Dahari (2016)
75	$CeNi_3Cr_2$	14.55	75.31	35	29.729	LT	Rusman and Dahari (2016)
76	MNi_5	20.92	96.65	35	32.219	LT	Kim et al. (1997)
77	MNi_5	20.92	96.77	35	32.705	LT	Huston (1980)
78	$V_{0.85}Cr_{0.15}$	29.71	125.52	35	33.629	LT	Kim et al. (1997)
79	$Ti_{0.99}Zr_{0.01}V_{0.43}Fe_{0.09}Cr_{0.05}Mn_{1.5}$	20.25	95.15	35	34.939	LT	Weckerle et al. (2019)
80	$Ca_{0.2}M_{0.8}Ni_5$	24.27	108.75	35	37.376	LT	Huston (1980)
81	$Ca_{0.2}M_{0.8}Ni_5$	24.27	108.78	35	37.542	LT	Kim et al. (1997)
82	$CeNi_5$	22.18	111.71	35	120.821	LT	Kim et al. (1997)

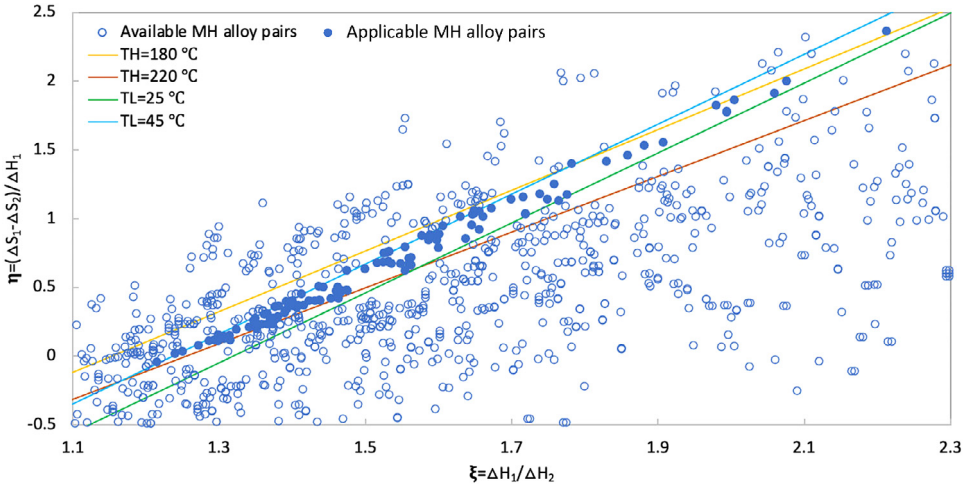

Fig. 3. Coordinate points (ξ, η) for the applicable MH alloys and four straight lines at maximum and minimum temperatures of T_h and T_l, and constant temperature T_m(=120°C).

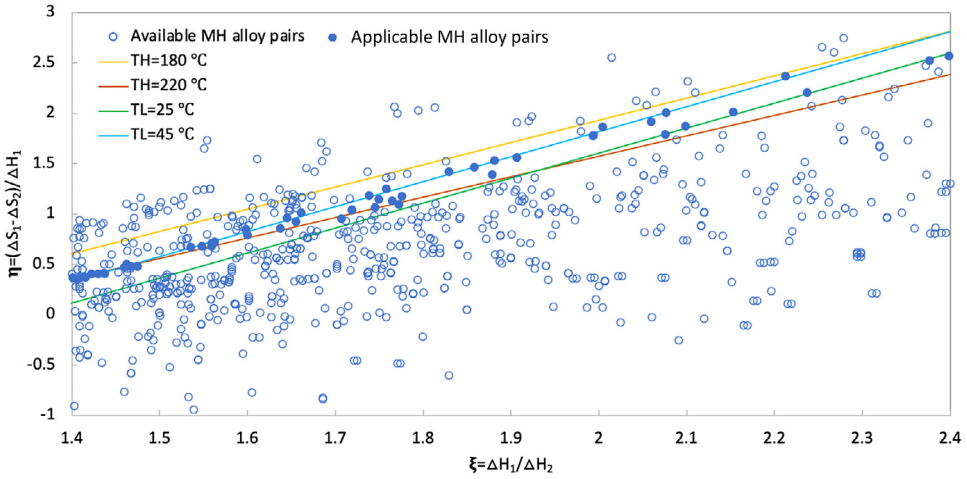

Fig. 4. Coordinate points (ξ , η) for the applicable MH alloys and four straight lines at maximum and minimum temperatures of T_h and T_l, and constant temperature T_m(=130°C).

be included and considered in the system energy calculation once the MH alloys are determined. The Cv_1 and Cv_2 are the specific heat capacity of MH alloys at constant volume for reactors MH1 and MH2 respectively. These MH alloy properties are important to calculate the energy inputs and outputs in the system but mostly are not available such that some modes of calculation correlations are necessarily generated. Henceforward, based on available data from literature, it is found that the specific heat capacity Cv is closely related to the molar mass of the MH alloy applied, as shown in Fig. 6. A linear correlation is therefore obtained to calculate the C_v with the function of molar mass of the MH alloy, if the data is not available:

$$C_v = 0.3995WM_{MH} + 33.287 \tag{13}$$

For this MHHP, the system efficiency is defined as coefficient of amplification (COA) and calculated as below:

$$COA = \frac{Q_{m1} + Q_{m2}}{Q_h} \tag{14}$$

Compared to conventional COP, the coefficient COA is of practical important for the specified application of hydride chemical heat pump (Grandjean et al., 1995). It should be noted that the LT heat source heat input Q_l is not taken into account in

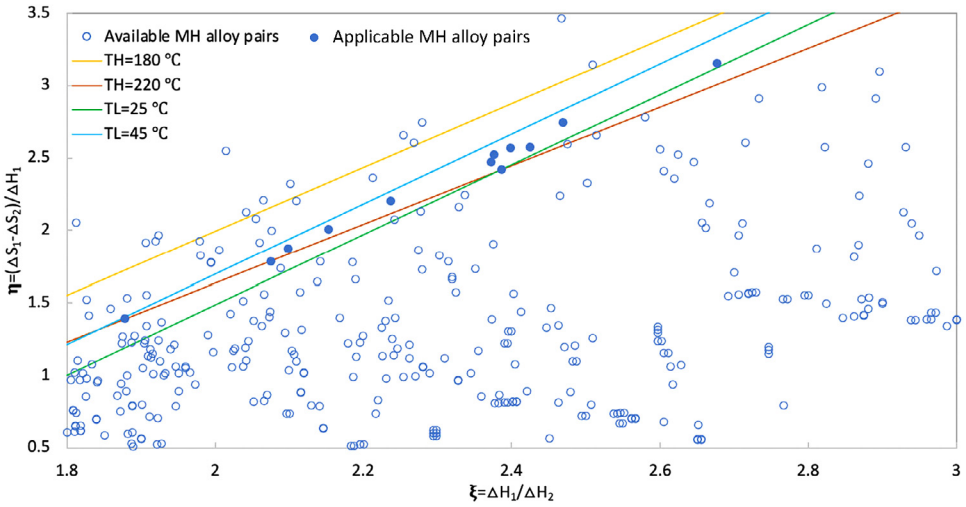

Fig. 5. Coordinate points (ξ , η) for the applicable MH alloys and four straight lines at maximum and minimum temperatures of T_h and T_l, and constant temperature T_m(=140°C).

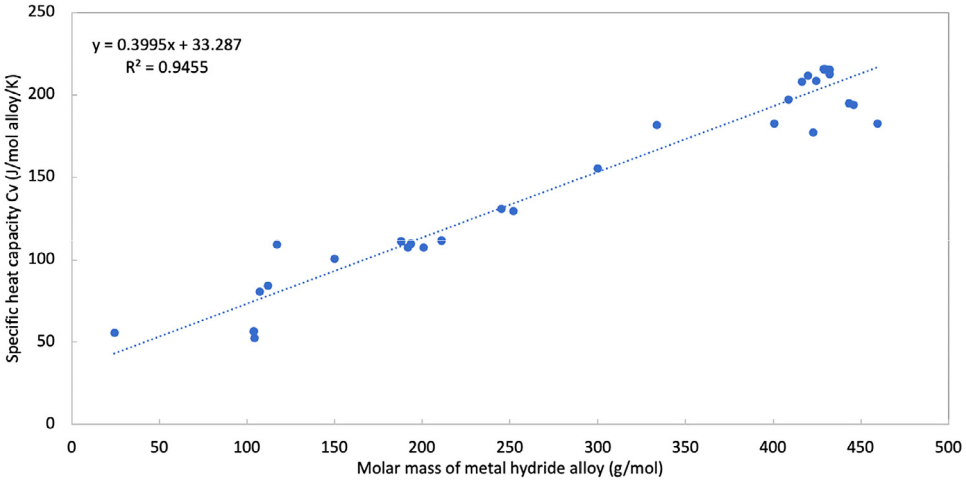

Fig. 6. Correlation of specific heat capacity at constant volume with molar mass for metal hydride alloys.

the calculation of COA since it is conventionally exhausted into ambient. Supposing all the system processes are reversible, the total entropy production during the system operation will be zero such that the Carnot coefficient of amplification COA_c can be derived and calculated as:

$$COA_c = \frac{T_m(T_h - T_m)}{T_h(T_m - T_l)} \tag{15}$$

The system exergy efficiency ψ can therefore be calculated as the ratio of COA and COA_c:

$$\psi = \frac{COA}{COA_C} \tag{16}$$

Based on the analysis results above, the applicable MH alloy pairs at heat output temperatures (T_m) 130 °C and 140 °C are listed in Tables 2 and 3 respectively. In addition, some important parameters including COA, COA_c, ψ, W_1, W_2, P_h, P_l, T_h and T_l are calculated and listed in each table, in which W_1 and W_2 are the weights of MH alloys charged in reactors MH1(MH1a or MH1b) and MH2 (MH2a or MH2b) respectively.

To evaluate and compare the system performance when different MH alloy pairs are applied, the variations of COA, COA_c and ψ with various MH alloy pairs at T_m temperatures of 130 °C and 140 °C are shown in Figs. 7 and 8 respectively. In addition, the variations of hydrogen high and low pressures with various MH alloy pairs at T_m temperatures of 130 °C and 140 °C are shown in Figs. 9 and 10 respectively. For the heat pump application, the system is applicable only if its system efficiency COA is higher than one. In that case, for the temperatures T_m at 130 °C and 140 °C, respectively 24 and 8 MH alloy pairs can be applied. For the high and low hydrogen pressures, the low hydrogen pressures are acceptable since almost all the low pressures are below 30 bar. However, some of the high pressures are quite high with the values up to 150 bar which need to be considered in the manufacturer's ability, cost and operating safety. As seen from Tables 2 and 3 and Figs. 7–10, only two MH alloy pairs can be applicable for both temperatures of T_m and acceptable COA values which are $LaNi_{4.25}Al_{0.75}$/ $Zr_{0.9}Ti_{0.1}Cr_{0.6}Fe_{1.4}$ (HT/LT) (pair number 6 in Table 2 and pair number 5 in Table 3) and $LaNi_{4.8}Al_{0.2}$/ $CeNi_3Cr_2$(HT/LT) (pair number 23 in Table 2 and pair number 9 in Table 3). However, the high hydrogen pressure with $LaNi_{4.8}Al_{0.2}$/$CeNi_3Cr_2$(HT/LT) is about 126 bar while the high hydrogen pressure with $LaNi_{4.25}Al_{0.75}$/ $Zr_{0.9}Ti_{0.1}Cr_{0.6}Fe_{1.4}$ is below 30 bar. Therefore, from the system performance point of view, the MH alloy pair of $LaNi_{4.25}Al_{0.75}$/ $Zr_{0.9}Ti_{0.1}Cr_{0.6}Fe_{1.4}$ is preferred.

Table 2
Applicable MH alloy pairs for T_m=130 °C.

Pair no	MH alloy pair		COA	COAc	ψ	W_1	W_2	P_h	P_l	T_h	T_l
	HT MH alloy	LT MH alloy	–	–	–	kg	kg	bar	bar	°C	°C
1	$LaNi_{4.6}Al_{0.4}$	$CeNi_3Cu_2$	0.969	1.421	0.682	0.59	1	51.122	9.853	202.04	23.20
2	$LaNi_{4.5}Al_{0.5}$	$Ce_{1.1}Ni_{2.5}Cu_{2.5}$	1.005	1.538	0.653	0.395	1	35.947	6.789	198.44	44.36
3	$LaNi_{4.6}Al_{0.4}$	$CeNi_{2.5}Cu_{2.5}$	1.019	1.464	0.696	0.589	1	56.178	9.853	206.95	26.55
4	$CaNi_5$	$CeNi_3Cu_2$	1.052	1.482	0.710	0.525	1	51.122	14.823	190.51	44.05
5	$LaNi_{4.7}Al_{0.3}$	$CeNi_{2.5}Cu_{2.5}$	1.110	1.499	0.741	0.441	1	56.178	15.518	188.77	48.06
6	$LaNi_{4.25}Al_{0.75}$	$Zr_{0.9}Ti_{0.1}Cr_{0.6}Fe_{1.4}$	1.258	1.532	0.821	1.96	1	25.079	2.646	212.56	32.42
7	$LaNi_{4.30}Mn_{0.70}$	$ZrCr_{0.6}Fe_{1.4}$	1.289	1.608	0.802	0.714	1	15.660	1.926	206.03	46.54
8	$LaNi_{4.75}Al_{0.25}$	$Ti_{0.98}Zr_{0.02}V_{0.41}Fe_{0.09}Cr_{0.05}Mn_{1.46}$	1.306	1.572	0.831	2.13	1	105.369	18.880	210.21	39.29
9	$LaNi_{4.5}Al_{0.5}$	$Zr_{0.8}Ti_{0.2}Cr_{0.6}Fe_{1.4}$	1.296	1.699	0.763	0.93	1	58.536	6.789	223.09	44.69
10	$LaNi_{4.7}Al_{0.3}$	$Ti_{0.98}Zr_{0.02}V_{0.41}Fe_{0.09}Cr_{0.05}Mn_{1.46}$	1.324	1.586	0.835	1.38	1	105.369	15.518	224.22	31.47
11	$LaNi_{4.5}Al_{0.5}$	$La_{0.6}Y_{0.4}Ni_{4.8}Mn_{0.2}$	1.325	1.703	0.778	0.867	1	56.311	6.789	221.04	46.27
12	$LaNi_{4.56}Mn_{0.44}$	$La_{0.6}Y_{0.4}Ni_{4.8}Mn_{0.2}$	1.326	1.685	0.787	0.698	1	56.311	6.342	221.70	44.15
13	$LaNi_{4.8}Al_{0.2}$	$Ti_{0.98}Zr_{0.02}V_{0.41}Fe_{0.09}Cr_{0.05}Mn_{1.46}$	1.357	1.569	0.865	1.25	1	105.369	23.342	198.23	48.21
14	$LaNi_{4.83}Mn_{0.17}$	$CeNi_4Zr$	1.441	1.611	0.894	3.85	1	140.580	22.112	218.26	38.39
15	$LaNi_{4.8}Al_{0.2}$	$CeNi_4Zr$	1.467	1.604	0.915	2.87	1	140.580	23.342	214.01	40.47
16	$LaNi_{4.61}Mn_{0.26}Al_{0.13}$	$La_{0.6}Y_{0.4}Ni_{4.8}Mn_{0.2}$	1.370	1.714	0.799	0.52	1	56.311	7.232	219.40	48.26
17	$LaNi_{4.61}Mn_{0.26}Al_{0.13}$	$Zr_{0.8}Ti_{0.2}Cr_{0.6}Fe_{1.4}$	1.340	1.710	0.784	0.56	1	58.536	7.232	221.47	46.68
18	$LaNi_{4.83}Mn_{0.17}$	$Ti_{0.98}Zr_{0.02}V_{0.41}Fe_{0.09}Cr_{0.05}Mn_{1.46}$	1.338	1.575	0.849	1.68	1	105.369	22.112	202.04	45.89
19	$LaNi_{4.8}Al_{0.2}$	$CeNi_4Cr$	1.342	1.477	0.909	2.50	1	129.697	23.342	209.49	26.44
20	$LaNi_{4.8}Al_{0.2}$	$Ti_{0.99}Zr_{0.01}V_{0.43}Fe_{0.09}Cr_{0.05}Mn_{1.5}$	1.318	1.567	0.842	1.22	1	145.585	23.342	215.99	34.53
21	$LaNi_{4.56}Mn_{0.44}$	$Zr_{0.8}Ti_{0.2}Cr_{0.6}Fe_{1.4}$	1.297	1.681	0.771	0.748	1	58.536	6.342	223.71	42.58
22	$LaNi_4Al$	$La_{0.6}Y_{0.4}Ni_{4.9}Al_{0.1}$	1.302	1.563	0.833	3.7	1	14.921	1.521	221.31	46.60
23	$LaNi_{4.8}Al_{0.2}$	$CeNi_3Cr_2$	1.301	1.417	0.919	2.713	1	125.899	30.032	207.85	35.55
24	$LaNi_4Al$	$ZrCr_{0.6}Fe_{1.4}$	1.177	1.564	0.752	2	1	15.660	1.078	223.38	29.19
25	$LaNi_{4.7}Al_{0.3}$	$CeNi_3Cu_2$	1.062	1.452	0.731	0.444	1	51.122	15.518	183.89	46.57
26	$LaNi_{4.61}Mn_{0.26}Al_{0.13}$	$Ce_{1.1}Ni_{2.5}Cu_{2.5}$	1.014	1.546	0.655	0.234	1	35.947	7.232	196.62	46.94
27	$LaNi_{4.65}Mn_{0.35}$	$CeNi_{2.5}Cu_{2.5}$	1.016	1.447	0.702	0.538	1	56.178	9.641	204.62	25.59
28	$LaNi_{4.56}Mn_{0.44}$	$Ce_{1.1}Ni_{2.5}Cu_{2.5}$	0.984	1.524	0.645	0.313	1	35.947	6.342	199.60	41.62

Table 3
Applicable MH alloy pairs for T_m=140 °C.

Pair no	MH alloy pair		COA	COAc	ψ	W_1	W_2	P_h	P_l	T_h	T_l
	HT MH alloy	LT MH alloy	–	–	–	kg	kg	bar	bar	°C	°C
1	$LaNi_{4.65}Mn_{0.35}$	$CeNi_3Cu_2$	0.954	1.405	0.679	0.54	1	57.100	12.669	205.44	35.69
2	$LaNi_{4.6}Al_{0.4}$	$CeNi_3Cu_2$	0.956	1.421	0.673	0.59	1	57.100	12.816	207.81	36.29
3	$LaNi_{4.65}Mn_{0.35}$	$CeNi_{2.5}Cu_{2.5}$	1.026	1.447	0.709	0.538	1	63.472	12.669	210.83	38.08
4	$LaNi_{4.6}Al_{0.4}$	$CeNi_{2.5}Cu_{2.5}$	1.030	1.464	0.703	0.589	1	63.472	12.816	213.47	38.63
5	$LaNi_{4.25}Al_{0.75}$	$Zr_{0.9}Ti_{0.1}Cr_{0.6}Fe_{1.4}$	1.139	1.532	0.743	1.96	1	29.740	3.644	220.22	43.32
6	$LaNi_{4.83}Mn_{0.17}$	$CeNi_4Cr$	1.310	1.482	0.884	3.35	1	146.246	28.372	220.57	35.47
7	$LaNi_{4.8}Al_{0.2}$	$CeNi_4Cr$	1.288	1.477	0.873	4.95	1	146.246	30.032	216.25	38.20
8	$LaNi_{4.83}Mn_{0.17}$	$CeNi_3Cr_2$	1.260	1.422	0.887	3.65	1	125.899	28.372	211.93	32.49
9	$LaNi_{4.8}Al_{0.2}$	$CeNi_3Cr_2$	1.245	1.417	0.879	5.41	1	125.899	30.032	207.85	35.55
10	$LaNi_{4.75}Al_{0.25}$	$CeNi_3Cr_2$	1.240	1.419	0.874	4.62	1	125.899	24.261	220.38	24.35
11	$Fe_{0.8}Ni_{0.2}Ti$	$CeNi_{2.5}Cu_{2.5}$	0.996	1.412	0.705	0.464	1	63.472	10.655	212.62	30.05
12	$Fe_{0.8}Ni_{0.2}Ti$	$CeNi_3Cu_2$	0.922	1.373	0.672	0.465	1	57.100	10.655	207.61	26.98

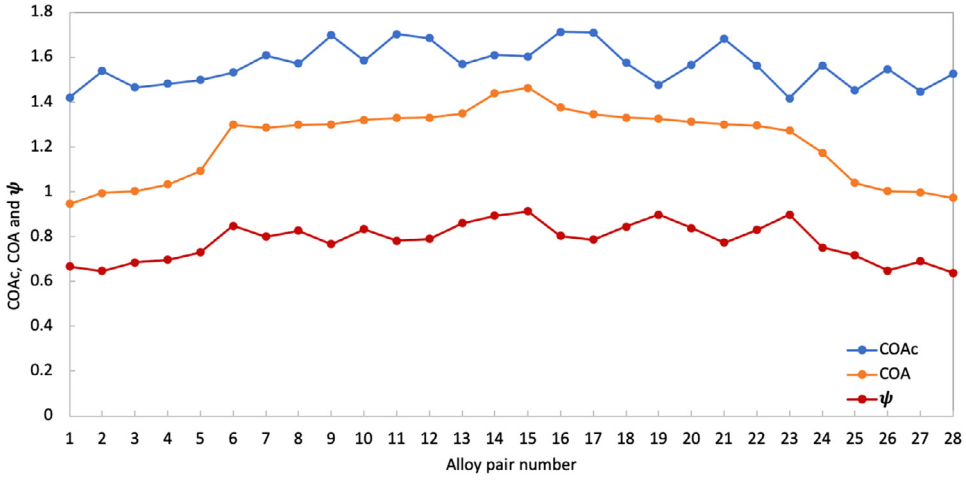

Fig. 7. Variation of COA, COA_c and ψ with different alloy pair numbers for T_m=130 °C.

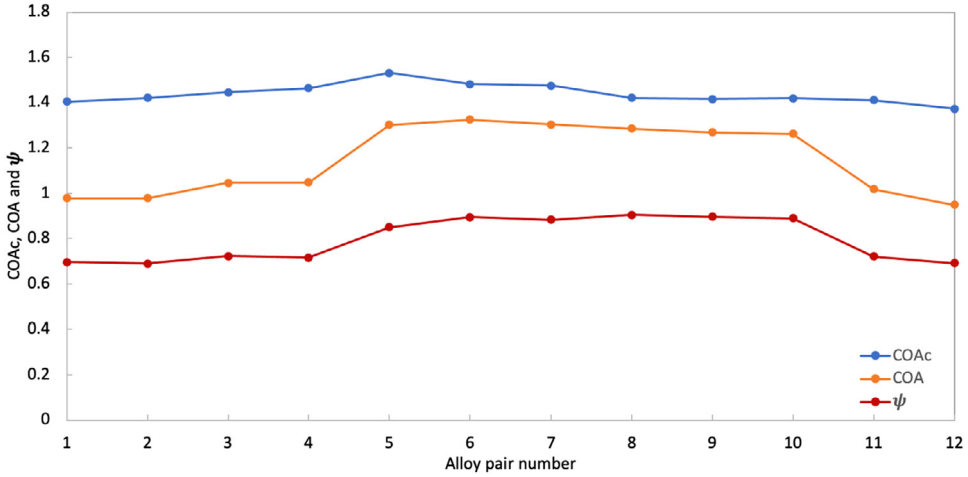

Fig. 8. Variation of COA, COA_c and ψ with different alloy pair numbers for T_m=140 °C.

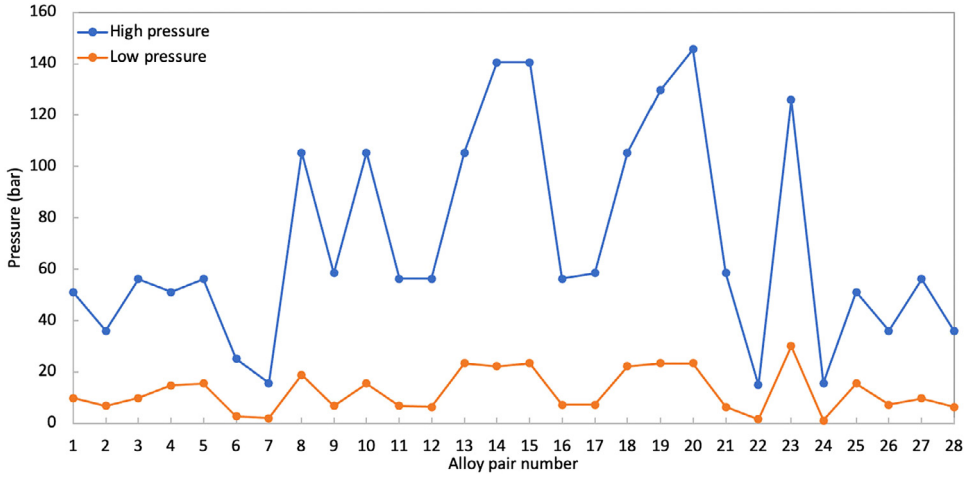

Fig. 9. Variation of high and low hydrogen pressures with different alloy pair numbers for T_m=130 °C.

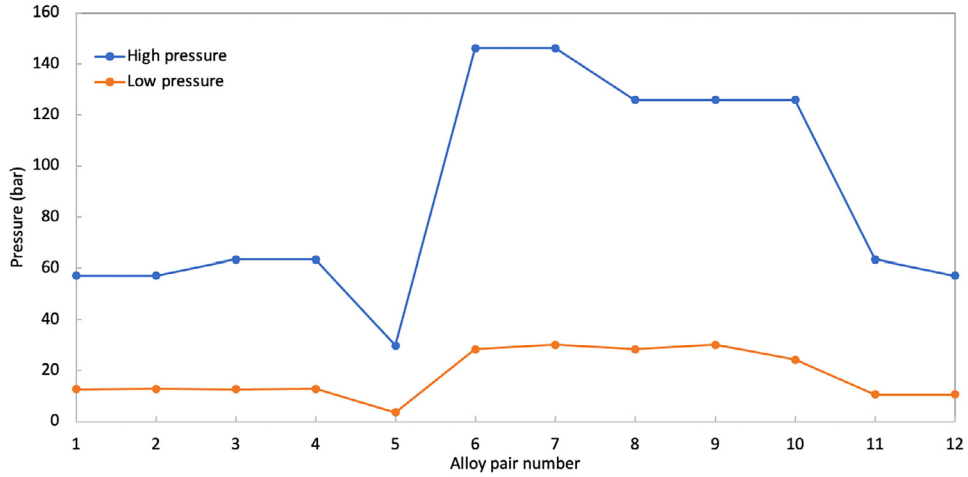

Fig. 10. Variation of high and low hydrogen pressures with different alloy pair numbers for T_m=140 °C.

3.3. System performance prediction

Based on the thermodynamic and operation analyses, the MH alloy pair $LaNi_{4.25}Al_{0.75}$/ $Zr_{0.9}Ti_{0.1}Cr_{0.6}Fe_{1.4}$(HT/LT) is determined for the proposed MHHP system. The system performance at different design and operating conditions can therefore be predicted. To simply the process, the effect of hysteresis on the MH absorption and desorption pressures at the same temperature is

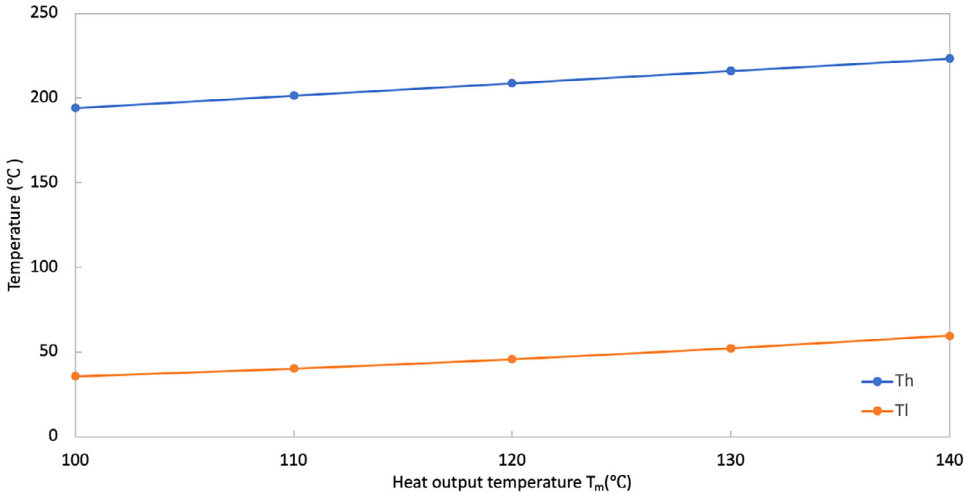

Fig. 11. Variation of high and low heat source temperatures (T_h and T_l) with heat output temperature T_m.

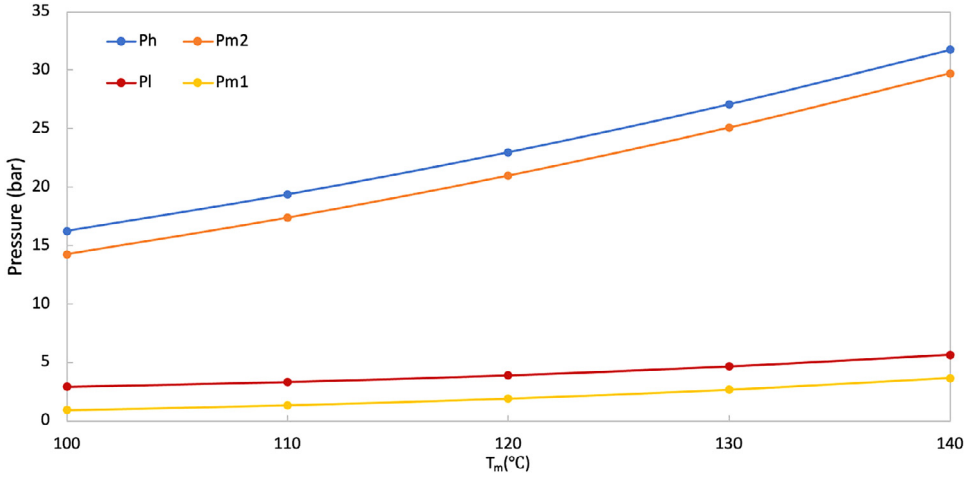

Fig. 12. Variation of high and low heat source temperatures (T_h and T_l) with heat output temperature T_m.

neglected. In addition, it is assumed that there is no temperature difference between heat source or sink temperature with its corresponding MH temperature. Nevertheless, effects of MH reactor heat capacity and hydrogen pressure difference for hydrogen transport through each MH rector pair are considered in the performance prediction. The metal material for each MH reactor is assumed as stainless steel and the meal reactor weight is assumed as 50% of its corresponding MH alloy charged. Since the weights of MH alloys in reactors MH1 and MH2 are 1.96 kg and 1 kg respectively, the corresponding reactor metal weights are 0.98 kg and 0.5 kg each. The hydrogen pressure difference between hydrogen transport through each MH rector pair on either high or low pressure side is assumed as 2 bar to facilitate the hydrogen transport. Accordingly, the variations of high and low temperature heat source temperatures T_h and T_l with heat output temperature T_m are calculated and shown in Fig. 11. It is seen from the prediction, the T_h and T_l both increase linearly with higher heat output temperature T_m. This indicates that to obtain a higher heat output temperature, both heat source temperatures of T_h and T_l need to be increased. Correspondingly, the variations of hydrogen pressures at those four reactors P_h, P_{m2}, P_{m1} and P_l with heat output temperature T_m are calculated and shown in Fig. 12. Similarly, the high and low side hydrogen pressures both increase with higher heat output temperature although the increase rates of the high side hydrogen pressures (P_h and P_{m2}) are relatively higher. This implies that the maximum MH reactor pressure should be considered at design stage based on the applicable maximum heat output temperature in the system. On the other hand, the system efficiencies in terms of COA_c, COA and ψ can be calculated at varied heat output temperatures as shown in Fig. 13. As depicted, the COA_c decreases with increased heat output temperature while the COA decreases slightly with higher heat output temperature. Subsequently the exergy efficiency ψ increases somewhat with the amplified heat output temperatures.

At constant heat output temperature T_m at 140 °C, the variations of low temperature heat input Q_l, heat output Q_m and system cycle time with high temperature heat input Q_h are calculated and demonstrated in Fig. 14. As depicted, both low temperature heat input Q_l and heat output Q_m increase with higher high temperature heat input Q_h. Meanwhile, the system cycle time decreases rapidly at the beginning and slows down a bit with the increased high temperature heat input. This indicates that at a designed heat output temperature, the heat output capacity, system cycle time and low temperature heat input can be controlled by the high temperature heat input.

4. Conclusions

There are plenty of low grade waste heat from industries which can be recovered and converted to useful heat for district

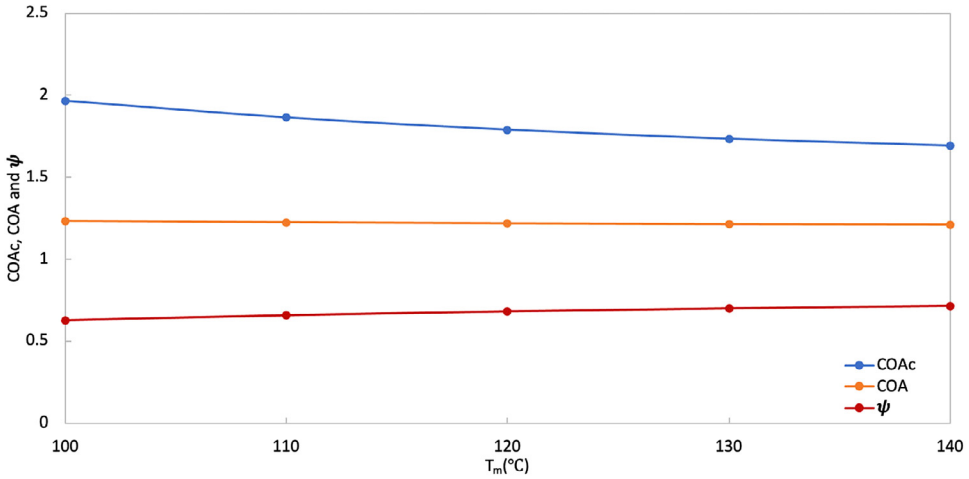

Fig. 13. Variation of COAc, COA, and Ψ with heat output temperature T_m.

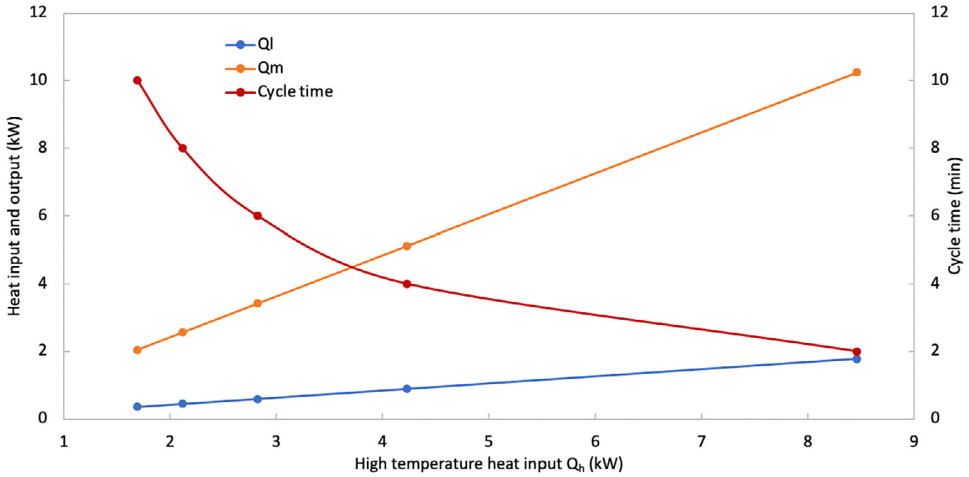

Fig. 14. Variation of low temperature heat input Q_l, heat output Q_m and cycle time with high temperature heat input Q_h.

heating network with the technology of metal hydride (MH) heat pump (MHHP). The MHHP has several advantages compared with other heat pump technologies. However, one of the important tasks to utilise this technology in the industrial waste heat recovery is to find out the appropriate MH alloys for the system. Therefore, in this paper, a detailed MH alloy selection procedures are explained for the proposed high temperature MHHP system. Of the total available MH alloys, an efficient method is proposed to classify the applicable high and low temperature MH alloys based on the lowest hydrogen operation temperature and its corresponding pressure. A number of MH alloy pairs can therefore be formed, and each MH pair consists of one high temperature alloy and one low temperature alloy. For these MH alloy pairs, thermodynamic analysis is conducted based on thermodynamic equilibrium in the system and specified operating conditions. The applicable MH pairs are therefore figured out for each designed heat output temperature. It is found that the higher the designed heat output temperature, the less the applicable MH pairs. Thereafter, operation analysis is carried out to evaluate and compare the system energy and exergy efficiencies and operating pressures at specified heat output temperatures. Meanwhile, a correlation to calculate alloy specific heat capacity at constant volume based on its molar mass is obtained which is quite useful for the operation analysis. The MH alloy pair for the proposed MHHP system is thus identified and finalised. The system performance is then predicted at various heat output temperatures and high temperature heat inputs. The predicted results can be applied for the optimal system designs and operation controls.

Declaration of competing interest

The authors declare that they have no known competing financial interests or personal relationships that could have appeared to influence the work reported in this paper.

Acknowledgement

The authors would like to acknowledge the support received from Research Councils UK (RCUK, EP/T022760/1) for this research project.

References

Anon, 2014. Element Energy- The potential for recovering and using surplus heat from industry. Final Report for DECC.

Bjurstrom, H., Suda, S., 1989. The metal hydride heat pump: dynamics of hydrogen transfer. Int. J. Hydrogen Energy 14, 19–28.

D. Chandra, D., Reilly, J.J., Chellappa, R., 2006. Metal hydrides for vehicular applications: The state of the art. JOM 58, 26–32.

Dantzer, P., Orgaz, E., 1986. Thermodynamics of hydride chemical heat pump-II. How to select a pair of alloys. Int. J. Hydrogen Energy 11, 797–806.

Gamnini, M., 1989. Performance of metal hydride heat pumps operation under dynamic conditions. Int. J. Hydrogen Energy 14, 821–830.
George, K., Cordin, A., Panagiotis, N., Stefan, B., 2020. Techno-economic analysis of high-temperature heat pumps with low-global warming potential refrigerants for upgrading waste heat up to 150 C. Energy Convers. Manage. 226, 113488.
Grandjean, F., Long, G.J., Buschow, K.H.J., 1995. Interstitial Intermetallic Alloys. Springer Netherlands, p. 728.
Huston, E.L., 1980. Engineering properties of metal hydrides. J. Less-Common Metals 74, 435–443.
Kim, K.J., Feldman Jr., K.T., Lloydt, G., Razanit, A., 1997. Compressor-driven metal-hydride heat pumps. Appl. Therm. Eng. 17, 551–560.
L. Li, L., Ge, Y.T., Luo, X., Tassou, S.A., 2017. Experimental investigations into power generation with low grade waste heat and R245fa organic rankine cycles (ORCs). Appl. Therm. Eng. 115, 815–824.
Lee, S.G., Kim, Y.K., Lee, J.Y., 1995. Operating characteristics of metal hydride heat pump using Zr-based laves phases. Int. J. Hydrogen Energy 20, 77–85.
Linder, M., Kulenovic, R., 2011. An energy-efficient air-conditioning system for hydrogen driven cars. Int. J. Hydrogen Energy 36, 3215–3221.
Linder, M., Laurien, E., 2009. Thermally driven sorption machine for fast hydrogen exchange. In: Proceedings of hydrogen and hydrogen storage – methods and materials. H3-2009, Indian Institute of Science, Bangalore, India, pp. 3–6.
Lototskyy, M.V., Tolj, I., Davids, M., Yevgeniy, V., Parsons, A., Swanepoel, D., et al., 2016. Metal hydride hydrogen storage and supply systems for electric forklift with low-temperature proton exchange membrane fuel cell power module. Int. J. Hydrogen Energy 41, 13831–13842.
Mellouli, S., Askri, F., Dhaou, H., Jemni, A., Nasrallah, S.B., 2009. Parametric studies on a metal hydride cooling system. Int. J. Hydrogen Energy 34, 3945–3952.
Muthukumar, P., Groll, M., 2010. Metal hydride based heating and cooling systems: A review. Int. J. Hydrogen Energy 35, 3817–3831.
Nakamura, H., Nakamura, Y., Fujitani, S., Yonezu, I., 1997. A method for designing a hydrogen absorbing laNi5-x-ymnxaly alloy for a chemical refrigeration system. J. Alloys Compd. 252, 83–87.
Ni, J., Liu, H., 2007. Experimental research on refrigeration characteristics of a metal hydride heat pump in auto air-conditioning. Int. J. Hydrogen Energy 32, 2567–2572.
Patsos, A., 2010. Port Talbot Exergy Mapping and waste heat recovery opportunities. Project Report 150552, Corus Research, Development & Technology.
Payá Herrero, J., 2010. Modelling and analysis of a metal hydride cooling system. (Ph.D. thesis). Valencia.
Qin, F., Chen, J., Lu, M., Chen, Z., Zhou, Y., Yang, K., 2007. Development of a metal hydride refrigeration system as an exhaust gas-driven automobile air conditioner. Int. J. Hydrogen Energy 32a, 2034–2052.
Qin, F., Chen, J., Lu, M., Chen, Z., Zhou, Y., Yang, K., 2007b. Development of a metal hydride refrigeration system as an exhaust gas-driven automobile air conditioner. Renew. Energy 32, 2034–2052.
Rusman, N., Dahari, M., 2016. A review on the current progress of metal hydrides material for solid-state hydrogen storage applications. Int. J. Hydrogen Energy 41, 12108–12126.
Satheesh, A., Muthukumar, P., 2010. Performance investigations of a single-stage metal hydride heat pump. Int. J. Hydrogen Energy 35, 6950–6958.
Skripnyuk, V.M., Ron, M., 1999. Evaluation of kinetics by utilizing the normalized pressure dependence method for the alloy $ti_{0.95}zr_{0.05}mn_{1.48}v_{0.43}fe_{0.08}al_{0.01}$. J Alloys Compd 293–295, 385–390.
Weckerle, C., Bu ̈ger, I., Linder, M., 2019. Numerical optimization of a plate reactor for a metal hydride open cooling system. Int. J. Hydrogen Energy 44, 16862–16876.
Yasuda, N., Tsuchiya, T., Okinaka, N., Akiyama, T., 2013. Application of metal hydride sheet to thermally driven cooling system. Int. J. Hydrogen Energy 38, 7469–7476.